Hybrid Proton Resonance Frequency Shift and Variable Flip Angle T_1 Temperature Mapping using a Golden-Angle 3D Stack-of-Radial Technique

Le Zhang[1], Tess Armstrong[1,2], Samantha Mikaiel[1,2], Alan Priester[3], Rory Geoghegan[4], Shyam Natarajan[3,4], and Holden H. Wu[1,2,4]

[1]Radiological Sciences, University of California Los Angeles, Los Angeles, CA, United States, [2]Physics and Biology in Medicine, University of California Los Angeles, Los Angeles, CA, United States, [3]Urology, University of California Los Angeles, Los Angeles, CA, United States, [4]Bioengineering, University of California Los Angeles, Los Angeles, CA, United States

Submission Category 1: 1201 Interventional: Thermotherapy & Thermometry
Submission Category 2: 902 Acquisition, Reconstruction & Analysis: Novel Acquisition – Encoding Methods, Trajectories & R…

Synopsis

Proton resonance frequency shift (PRF) is widely used for MR temperature mapping, but is not applicable in adipose tissues. T_1 measurement is an alternative MR temperature mapping method that can be applied in adipose tissues. Combined PRF-T_1 mapping has been evaluated for Cartesian MRI, but there is a lack of research for non-Cartesian techniques. In this work, we propose a new multi-echo 3D stack-of-radial technique that combines PRF and variable-flip-angle T_1 measurement for MR temperature mapping. Preliminary results from laser ablation in phantoms demonstrate good agreement between temperature derived from both PRF and T_1 compared to readings of temperature probes.

Introduction

Proton resonance frequency shift (PRF) is a widely used method for MR temperature mapping. However, PRF fails in adipose tissue due to the absence of hydrogen bonds. Alternatively, T_1 relaxation time has been used to measure temperature in adipose tissues using variable flip-angle (VFA) gradient-recalled echo (GRE) imaging. Combined PRF-T_1 methods have been investigated for Cartesian sampling (1,2), but there is a lack of research for non-Cartesian sampling. Non-Cartesian sampling schemes such as golden-angle 3D stack-of-radial offer inherent robustness to motion and potential for accelerating acquisition speed (3). In this abstract, we propose a new golden-angle 3D stack-of-radial MRI technique that combines PRF and VFA T_1 measurement for temperature mapping. Proof-of-concept phantom ablation experiments are presented to evaluate the feasibility and accuracy of this new method.

Methods

Hybrid PRF-T_1 3D Stack-of-Radial Temperature Mapping

Fig. 1 shows the proposed method based on a bipolar multi-echo RF-spoiled GRE sequence with the golden-angle-ordered 3D stack-of-radial trajectory (4). Parameters are presented in **Table 1**. The magnitude images of the first echo acquired using both flip

angles are used for T_1 mapping **(Fig.1b)**, while the echo-combined phase images acquired with the larger flip angle are used for PRF temperature mapping **(Fig.1c)**. To correct for eddy current effects and gradient errors, 80 calibration spokes (40 each for G_x and G_y) were obtained in a reference scan (5).

Phantom Experiments

Focal laser ablation (PhoTex15, BioTex) was performed at 3T (Prisma, Siemens) in a gel phantom, which was kept in a 37°C water bath prior to the experiment. A laser fiber was inserted into the phantom and a temperature probe was inserted in parallel to measure real-time temperature change as reference. The two optimal flip angles for VFA were calculated for an expected phantom T_1 of 2.5s to be 2° and 12°. A B_1+ map was acquired to calibrate the flip angles. The proposed sequence was first run at baseline (37°C) to provide a reference before 30 measurements were obtained during ablation. Data acquired from all channels were adaptively combined (6). For PRF thermometry, all echoes were combined (3) with an effective TE of 10ms. Temperature change was extracted from the evolution of both the phase of the combined echo with a coefficient of -0.01ppm/°C, and the T_1 map with the coefficient of 5.76ms/°C (7) using the standard VFA fitting process (8). For T_1 maps, the amplitude images of three consecutive acquisitions were averaged in a sliding-window approach to improve SNR.

Results

Fig.2a shows the magnitude image of the central coronal slice at baseline. The paths of the laser fiber and temperature probe are represented by the red and white lines, respectively. **Fig.2c** and **Fig.2d** show the relative temperature change with respect to baseline temperature using PRF at the time of peak temperature and at the end of ablation, respectively. In both images, the white cross marks the position of one temperature sensor, whose readings are shown in **Fig.2b** along with the absolute PRF temperature value of the corresponding pixel.

Fig.3 shows the T_1 maps of the central coronal slice using the proposed sequence at the baseline temperature, at the time of peak temperature and at the end of ablation. **Fig.3d** illustrates the change in T_1 value at peak temperature with respect to **Fig.3a**. In **Fig.3e** the change in T_1 value in the pixel marked by the cross is translated to absolute temperature values, which are plotted alongside the temperature probe readings.

Discussion

The proposed sequence achieved spatial coverage of $112\times112\times50mm^3$ with resolution of 1.2mm and temporal resolution of 10s per dataset. The PRF results obtained in the laser ablation experiment showed a high degree of agreement with temperature probe readings. An average deviation of 2°C was observed between the PRF and temperature probe results, likely attributable to the low SNR and the high radial undersampling. The T_1 measurement, however, was much noisier and yields, on average, 4.5°C lower temperature values. This can be due to several factors. First, the expected T_1 time (2.5s) used in determining the optimal flip angles was very different from the T_1 measured (~1.2s). Second, the small number of radial spokes might not establish GRE steady-state for VFA. Lastly, the temperature coefficient for water T_1 is known to vary and can cause an error of ~10°C. These can be better addressed when the proposed

sequence is applied to adipose tissues, whose shorter T_1 and better characterized temperature coefficient can lead to higher SNR and temperature accuracy. Future work will include the incorporation of parallel imaging and constrained reconstruction to achieve higher coverage, finer spatiotemporal resolution, and increased temperature accuracy.

Conclusion

We proposed a new hybrid PRF-T_1 thermometry method using the golden-angle 3D stack-of-radial trajectory. Preliminary data using this technique demonstrated promising temperature accuracy with dynamic 3D coverage.

ACKNOWLEDGEMENTS
The authors thank Dr. Xiaodong Zhong at Siemens Healthineers for helpful discussions. This work was supported in part by Siemens Healthineers.

REFERENCES
1. Todd N, Diakite M, Payne A, Parker DL. Hybrid proton resonance frequency/T1 technique for simultaneous temperature monitoring in adipose and aqueous tissues. Magn. Reson. Med. [Internet] 2013;69:62–70. doi: 10.1002/mrm.24228.
2. Todd N, Diakite M, Payne A, Parker DL. In vivo evaluation of multi-echo hybrid PRF/T1 approach for temperature monitoring during breast MR-guided focused ultrasound surgery treatments. Magn. Reson. Med. [Internet] 2014;72:793–799. doi: 10.1002/mrm.24976.
3. Svedin BT, Payne A, Bolster BD, Parker DL. Multiecho pseudo-golden angle stack of stars thermometry with high spatial and temporal resolution using k-space weighted image contrast. Magn. Reson. Med. [Internet] 2017:1–13. doi: 10.1002/mrm.26797.
4. Winkelmann S, Schaeffter T, Koehler T, Eggers H, Doessel O. An Optimal Radial Profile Order Based on the Golden Ratio for Time-Resolved MRI. IEEE Trans. Med. Imaging [Internet] 2007;26:68–76. doi: 10.1109/TMI.2006.885337.
5. Armstrong T, Dregely I, Stemmer A, Han F, Natsuaki Y, Sung K, Wu HH. Free-breathing liver fat quantification using a multiecho 3D stack-of-radial technique. Magn. Reson. Med. [Internet] 2017:1–13. doi: 10.1002/mrm.26693.
6. Walsh DO, Gmitro AF, Marcellin MW. Adaptive reconstruction of phased array MR imagery. Magn. Reson. Med. [Internet] 2000;43:682–690. doi: 10.1002/(SICI)1522-2594(200005)43:5<682::AID-MRM10>3.0.CO;2-G.
7. Hey S, de Smet M, Stehning C, Grüll H, Keupp J, Moonen CTW, Ries M. Simultaneous T1 measurements and proton resonance frequency shift based thermometry using variable flip angles. Magn. Reson. Med. [Internet] 2012;67:457–463. doi: 10.1002/mrm.22987.
8. Fram EK, Herfkens RJ, Johnson GA, Glover GH, Karis JP, Shimakawa A, Perkins TG, Pelc NJ. Rapid calculation of T1 using variable flip angle gradient refocused imaging. Magn. Reson. Imaging [Internet] 1987;5:201–208. doi: 10.1016/0730-725X(87)90021-X.
9. Jonathan S V., Grissom WA. Volumetric MRI thermometry using a three-dimensional stack-of-stars echo-planar imaging pulse sequence. Magn. Reson. Med. [Internet] 2017:1–11. doi: 10.1002/mrm.26862.

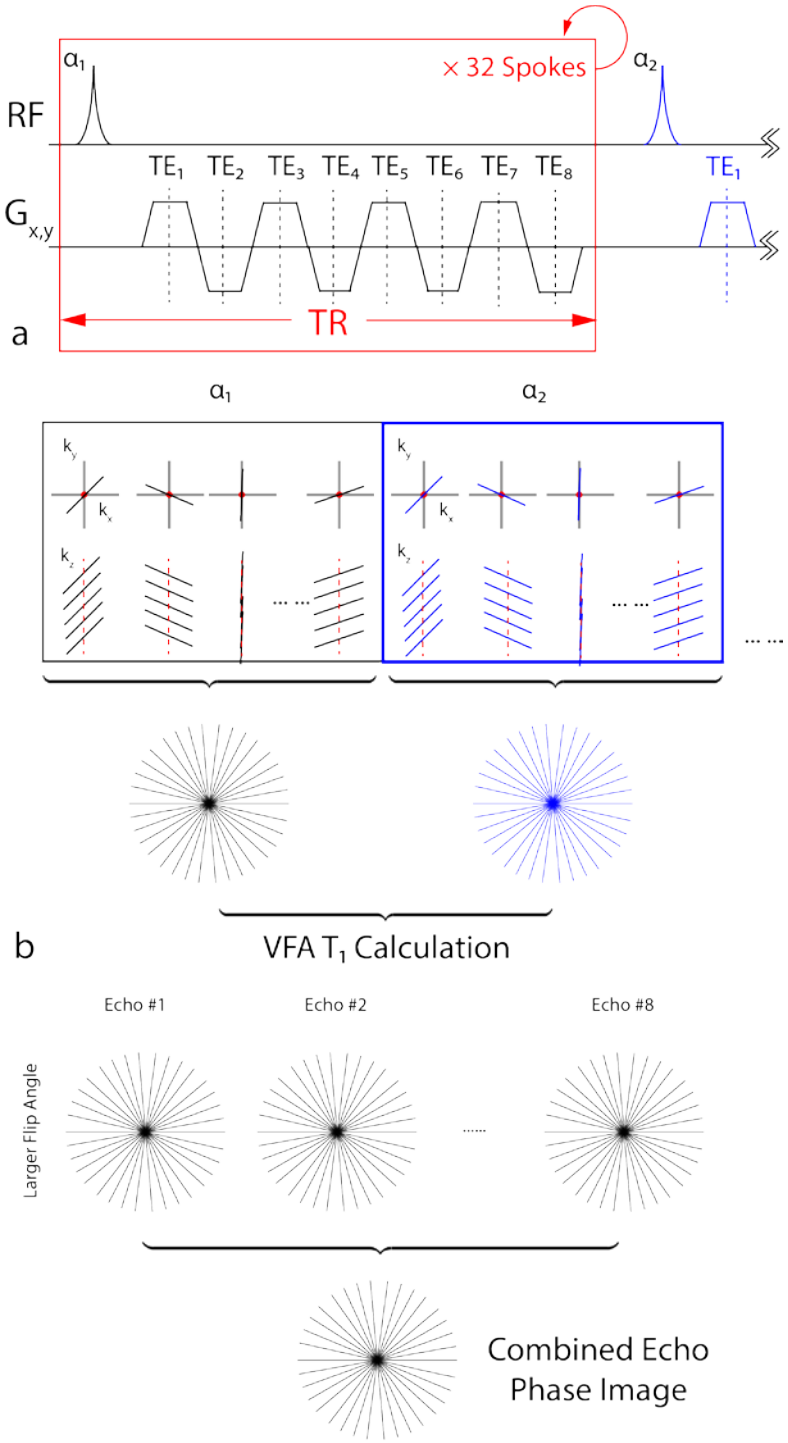

Figure 1: Schematics of the 3D stack-of-radial hybrid proton resonance frequency shift (PRF) and T_1 thermometry method. **(a)** Variable flip angle (VFA) multi-echo radial pulse sequence diagram. **(b)** The first echoes of all 32 radial spokes were combined for each flip angle before VFA calculation was carried out. **(c)** The eight echoes acquired with the larger flip angle (α_1) were combined, the phase images of which were used to calculate PRF temperature change.

Imaging Parameters	Radial Sequence
Minimal TE (ms)	1.42
ΔTE (ms)	1.27
Number of Echoes	8
TR (ms)	13.8
Matrix	96×96×10
FOV (mm×mm×mm)	112×112×50
Resolution (mm×mm×mm)	1.2×1.2×5
Slice Thickness (mm)	5
Radial Spokes	32
Flip Angles	2° & 12°
Bandwidth (Hz/pixel)	1150
Acceleration Factor (R)	8
Scan Time (Both FAs) (s)	10*

Table 1: Sequence parameters used in the ablation experiment. *The gradient calibration time in the baseline image at 37°C is excluded.

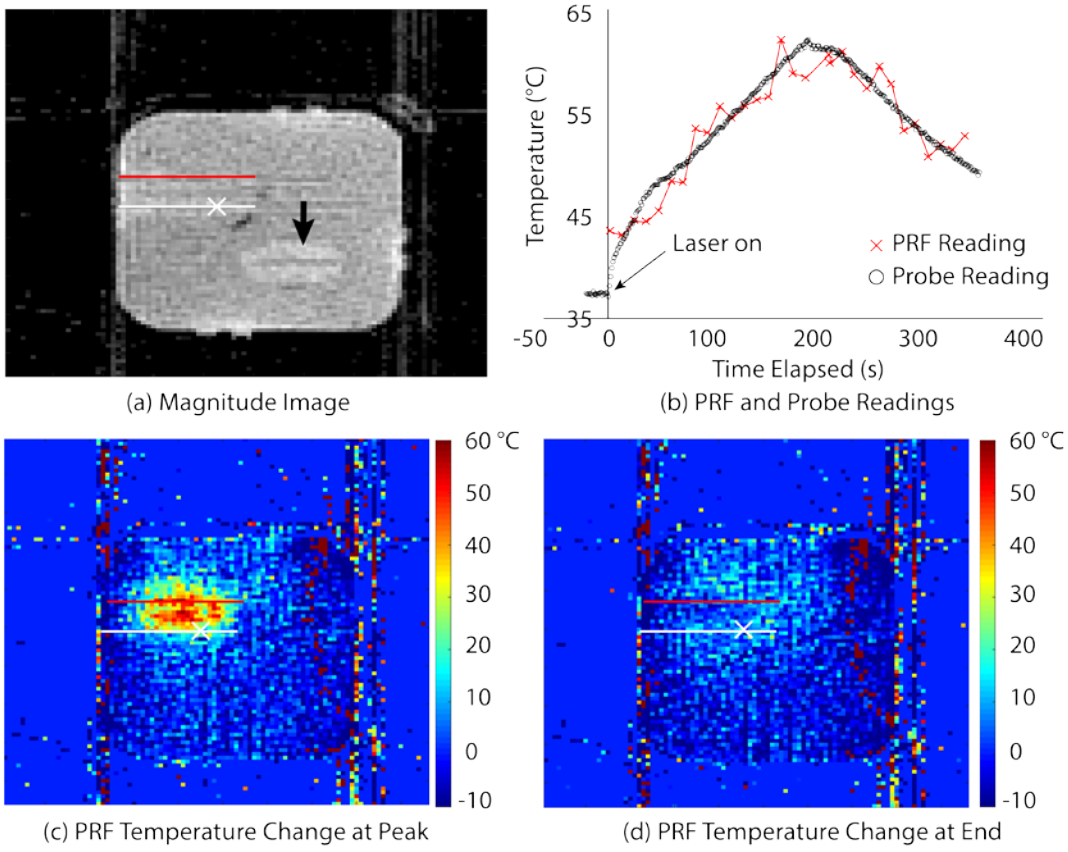

Figure 2: (a) Baseline coronal magnitude image before ablation. The white and red lines show, respectively, the paths of the temperature probe and laser fiber. The black arrow points to a region which was previously ablated. **(b)** Plot of the PRF temperature and the reading of one sensor on the temperature probe marked by the cross in **(a)**. **(c&d)** Temperature change maps calculated from PRF with respect to baseline at peak

temperature and at the end of ablation, respectively.

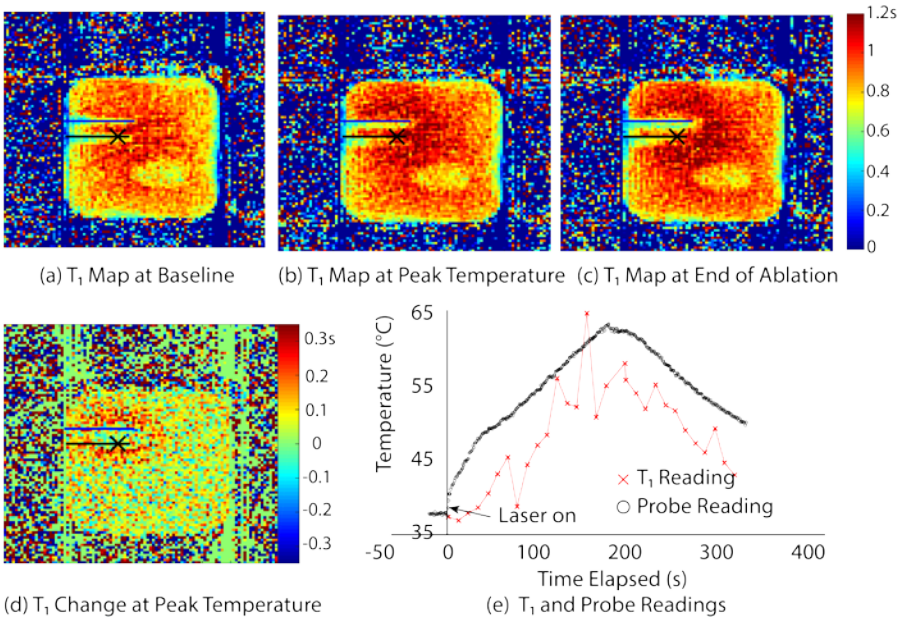

Figure 3: (a~c) The coronal T_1 map at baseline temperature, peak temperature, and the end of ablation. **(d)** The change in T_1 value at peak temperature with respect to the baseline. **(e)** Plot of the temperature sensor reading (position marked by the black cross) and T_1 thermometry results during ablation.